Supporting Information

Visible-light-responsive Z-scheme system for photocatalytic lignocelluloses-to-H_2 conversion

Qing-Yu Liu,[a,‡] Hao-Dong Wang, [a,‡] Yong-Jun Yuan,*[a] Rui Tang, Liang Bao,[a] Zhanfeng Ma,[a] Jiasong Zhong ,[a] Zhen-Tao Yu,*[b] and Zhigang Zou [b]

[a]College of Materials and Environmental Engineering, Hangzhou Dianzi University, Hangzhou, 310018, People's Republic of China.

E-mail: yjyuan@hdu.edu.cn; zhang@hdu.edu.cn

[b]National Laboratory of Solid State Microstructures and Collaborative Innovation, Center of Advanced Microstructures, Jiangsu Key Laboratory for Nano Technology, College of Engineering and Applied Science, Nanjing University, Nanjing 210093, People's Republic of China

E-mail: yuzt@nju.edu.cn.

‡These authors contributed equally to this work.

Experiment section

Materials

All chemical reagents are of analytic grade and were used as received without further purification.

Synthesis of $CoTiO_3$ nanorods

The $CoTiO_3$ nanorods was synthesized via a simple precipitation process. Firstly, 0.01 mol $Co(CH_3COO)_2{\cdot}4H_2O$ and 3.4 ml $Ti(OC_4H_9)_4$ were dispersed in 60 ml ethylene glycol (EG) and formed burgundy solution. Then, the burgundy solution would change into light ping suspension after 8 h magnetic stirring under room temperature. The light pink precipitate was separated from mixture solution and washed with alcohol for three times. After drying under vacuum, the precursor was heated up to 700 ℃ with a heating rate of 2 ℃·min^{-1} for 4 h to obtain green $CoTiO_3$ nanorods sample.

Synthesis of CdS

The CdS nanoparticles were synthesized by a hydrothermal method. Firstly, 160 ml 0.14 M Na_2S solution was added slowly to 200 ml 0.14 M $Cd(OAc)_2$ aqueous solution. After keeping violently stirring for 24 h and laying aside 24 h, the resulting yellow precipitate was separated by filtration. And then, the product dispersed in water was transferred into Teflon-lined stainless-steel autoclave (30 ml), which was heated to 473 K for 72 h. The resulted solution was cooled to room temperature, the yellow CdS was collected by centrifugation and then washed with deionized water and alcohol, and dried in vacuum oven for 24 h at room temperature.

Synthesis of CdS/Pt

The CdS/Pt was obtained via a simple photo-deposition process. In a typical experimant, a certain percentage of K_2PtCl_4 was added into and 250 ml aqueous solution consisting of 0.5 CdS, and then irradiated with 300W Xe lamp for 2 h. The precipitate was collected by centrifugation and washed with ethanol and water for three times. Finally, the product was dried in a vacuum oven overnight at room temperature. The weight ratio of Pt loaded on the CdS at the following values: 1%, 2%, 3%, 4%, and 5%.

Synthesis of $[Co(bpy)_3]^{3+}$ and $[Co(bpy)_3]^{2+}$

1 g $CoCl_2 \cdot 6H_2O$ and 2.2 g 2,2'-bipyridyl were dissolved in 100 ml of methanol to form mixture solution, and then the solution was refluxed at 60 ^oC. After the solution was cooled down to room temperature, 3.4 g NH_4PF_6 was added into solution and stirred for 30 mins to form yellow precipitate. The product was collected by centrifugation and dried in a vacuum oven overnight. To prepare $[Co(bpy)_3](PF_6)_3$ complex, 500 mg $[Co(bpy)_3](PF_6)_2$ (500 mg) and 107 mg $NOBF_4$ were added to 15 ml of acetonitrile solution and stirred for 0.5 h, and then the solvent was evaporated, the resulted residue was dissolved in 5 ml of acetonitrile. After 502 mg NH_4PF_6 was added into the mixture solution, $[Co(bpy)_3](PF_6)_3$ was obtained as a precipitate which was filtered and then dried in a vacuum oven at room temperature for 12 h.

Photocatalytic H_2 production experiments

The photocatalytic H_2 production experiment was carried out an outer irradiation Pyrex photoreactor with a top window connected to a closed gas-circulating system.

Typically, CdS (50 mg), $CoTiO_3$ (50 mg), $[Co(bpy)_3](PF_6)_2$ (20mg), $[Co(bpy)_3](PF_6)_3$ (20mg) and cellulose (1 g) were dispersed in 250 ml of neutral aqueous solution, and the mixture solution was stirred for 20 minutes. Meanwhile, the system was thoroughly degassed to avoid the interference of the dissolved air completely. Then solution was irradiated by a 300 W Xenon lamp equipped with cutting-off filter (λ > 420 nm), and the generating H_2 amount was analyzed by an on-line gas chromatography (CG1690, Jiedao, TCD) using a 5 Å molecular sieves column and argon as the carrier gas. The temperature of photocatalytic system maintained at room temperature by using a flow of cooling water during the photocatalytic reaction. The apparent quantum efficiency (AQY) of photocatalytic H_2 evolution system was measured under monochromatic light illumination, and the AQY was calculated according to the following equations:

$$n_{\text{photons}} = \frac{P\lambda}{hc} \times t \qquad (1)$$

$$\text{AQY}[\%] = \frac{\text{number of reacted electrons}}{\text{number of incident photons}} \times 100$$

$$= \frac{2 \times \text{number of evolved } H_2 \text{ molecules}}{\text{number of incident photons}} \times 100 \qquad (2)$$

where P, λ, h, c and t is the input optical power, wavelength of the light, Planck's constant, speed of light and the illumination time, respectively.

Structural characterization

Powder X-ray diffraction was performed with a Rigaku-miniflex6 X-ray diffractometer operating at 40 kV and 15 mA with Cu Kα radiation (λ = 0.15406 nm), recorded with 2θ ranging from 10 to 80° with a scan rate of 10° min^{-1}. Scanning

electron microscope(SEM) and transmission electron microscopy (TEM) images of samples were recorded using a Carl Zeiss Gemini vltra55 microscopy and JEOL JEM 2010 microscopy, respectively. The SEM and TEM samples were prepared by drop-casting dispersion onto a silicon wafer and carbon grid, respectively. UV–vis diffused reflectance spectra of all samples were recorded on a Beijing Purkinje TU-1901 spectrophotometer (China) equipped with a lab-integrating sphere diffuse reflectance accessory, using $BaSO_4$ as a reflectance standard. The specific surface area was discussed from the N_2 adsorption/desorption isotherms by the Brunauer-Emmett-Teller (BET) method on a Quanta chrome Quadrasorb SI porosimeter. X-ray photoelectron spectroscopy (XPS) analysis was performed on a VG ESCALAB MKII X-ray photoelectron spectrometer using monochromatic Al Kα radiation, and whole the binding energies were calibrated, based on the C1s peak at 284.8eV as the reference. Fluorescence spectra were recorded on an Edinburgh FS1 fluorescence spectrophotometer. The transient photocurrent was measured in 0.5 M Na_2SO_4 aqueous solution with a standard three-electrode system that consists of a sample-coated ITO glass as the working electrode, a saturated Ag/AgCl electrode as the reference electrode and a Pt wire as the counter electrode driven by electrochemical workstation (CHI660E, Shanghai Chenhua Limited, China) with an external voltage of 0.5 V vs. RHE with a rate of 100 $mV \cdot S^{-1}$. An electrophoretic deposition (EPD) method was used to prepare the sample coated ITO glass electrode. The EPD experiment was conducted on two parallel ITO glass with the distance of 1 cm in 25 ml acetone solution consisting of 10 mg sample under an external voltage of 8 V for 5 min. The

cyclic voltammetry was measured by the same method a standard three-electrode system as above-mentioned expect by using sample-coated glassy carbon (GC) as the working electrode. For the CO_2 detection, 1ml CO_2 extracted from the photocatalytic reaction system was detected by carbon dioxide analyzer (AR8200, Smart Seneor, China). The organic product was analyzed by Agilent 8860-5977B gas chromatography-mass spectrometer (GC-MS) equipped with aDB-5MS column. The high performance liquid chromatography analysis was performed on a Shimadzu HPLC LC-20AD system equipped with a Xtimate C18 column. 0.05 M KH_2PO_4 solution was used as the mobile phase that had a flow rate of 1 $mL \cdot min^{-1}$. The column temperature was 30 ^oC. The amount of product was determined by using calibration curves.

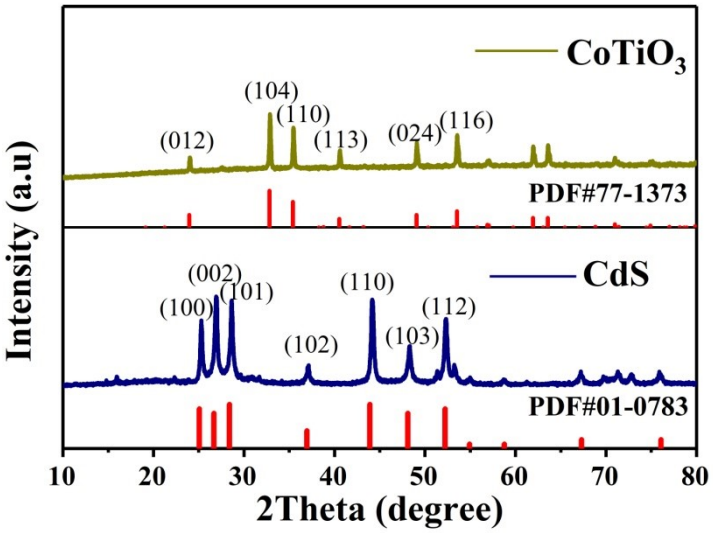

Figure S1. XRD patterns of CdS and $CoTiO_3$.

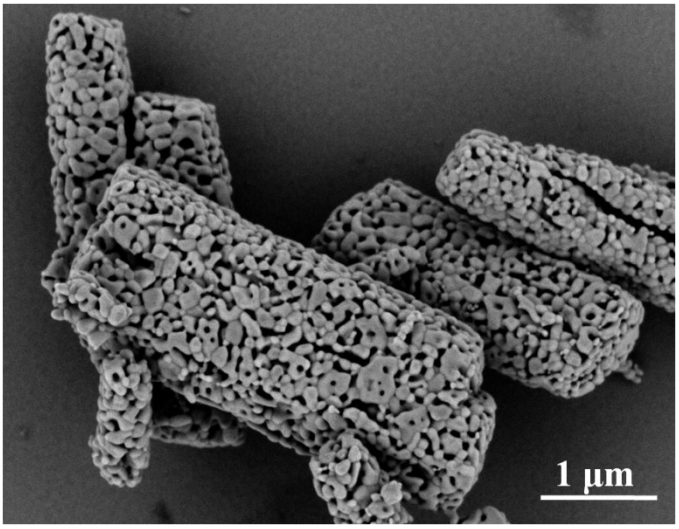

Figure S2. SEM image of $CoTiO_3$.

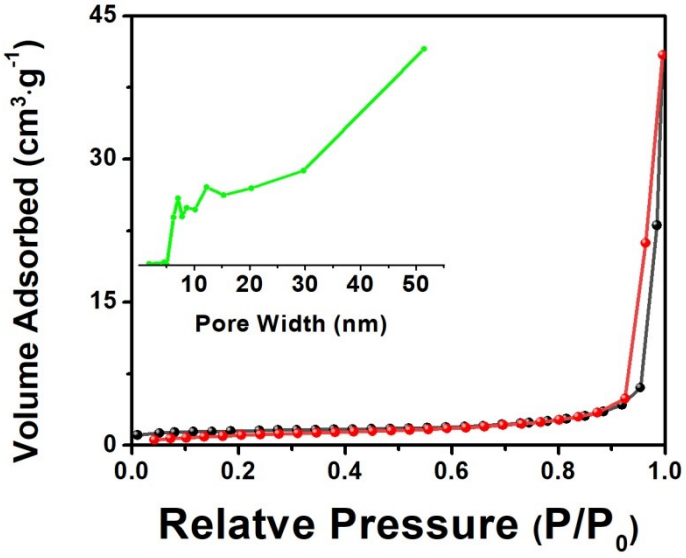

Figure S3. N_2 absorption-desorption isotherm and corresponding pore size distribution (inset) of $CoTiO_3$. The pore size of $CoTiO_3$ calculated from the desorption branch of the nitrogen isotherm was observed to be 15.2 nm.

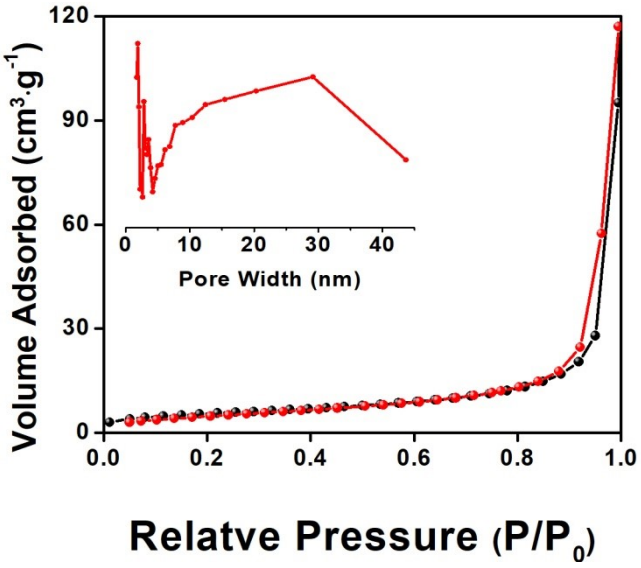

Figure S4. N_2 absorption-desorption isotherm and corresponding pore size distribution (inset) of CdS nanoparticles. The pore size of CdS calculated from the desorption branch of the nitrogen isotherm was observed to be 12.8 nm.

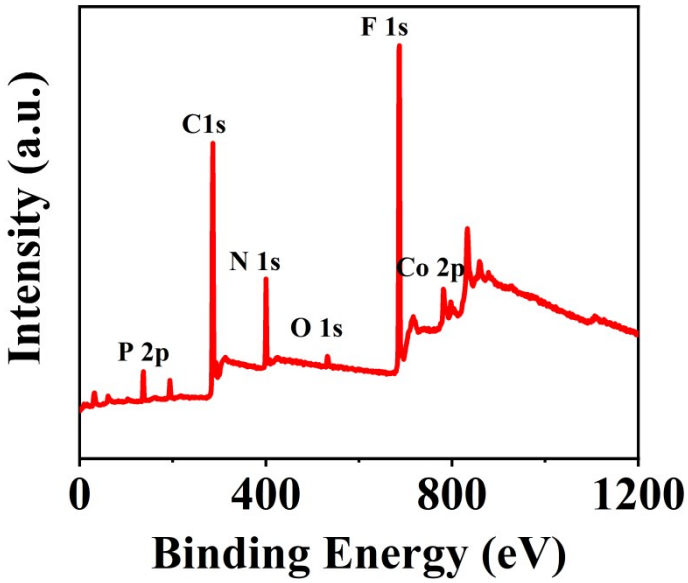

Figure S5. Wide XPS spectrum of $Co(bpy)_3^{2+}$ and $Co(bpy)_3^{2+}$.

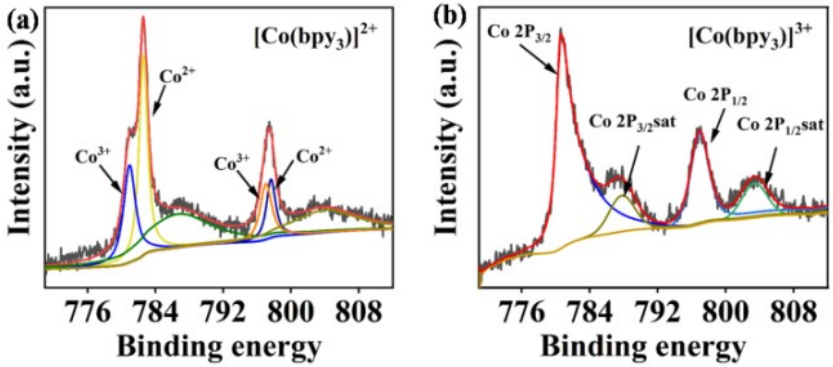

Figure S6. (a) high-resolution Co 2p XPS spectrum of $[Co(bpy)_3]^{2+}$, (b) high-resolution Co 2p XPS spectrum of $[Co(bpy)_3]^{3+}$. The high-resolution XPS spectra of Co $2P_{3/2}$ spectrum can be deconvoluted into two spin-orbit doublet peaks of Co^{2+} and Co^{3+}, located at 782.5 eV and 780.9 eV, indicating that there were a small quantity of Co^{3+} formed during the preparation process of $[Co(bpy)_3]^{2+}$. As for the $[Co(bpy)_3]^{3+}$ sample, four peak at 780.2, 786.4, 796.8 and 804.3 eV was observed in the high-resolution XPS Co 2p spectra shown in Figure 2b, which can be attributed to Co $2p_{3/2}$, Co $2p_{3/2}$(sat), Co $2p_{1/2}$, Co $2p_{1/2}$(sat), respectively. Obviously, only Co^{3+} peaks were found in the complex, suggesting the successful oxidation of $[Co(bpy)_3]^{2+}$ to $[Co(bpy)_3]^{3+}$.

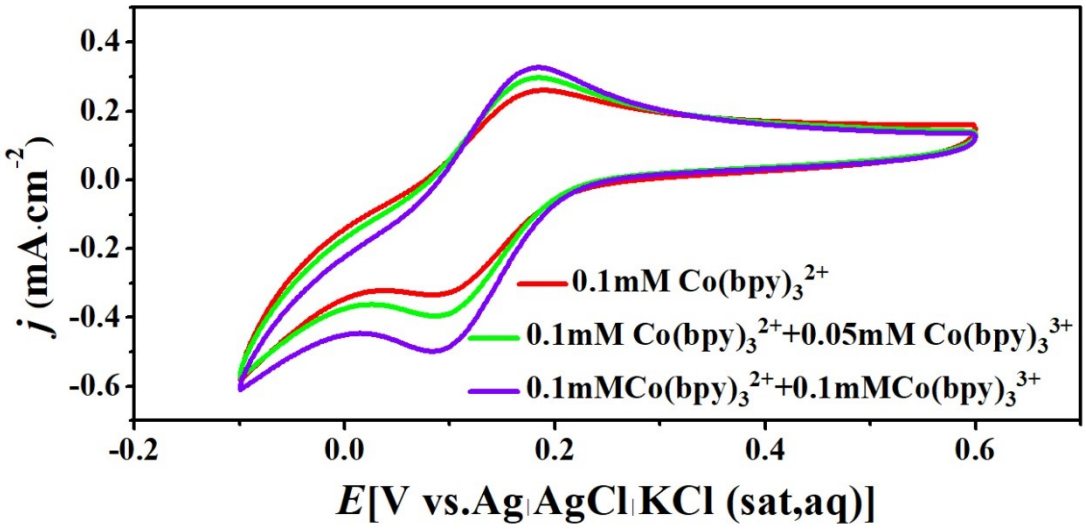

Figure S7. Cyclic voltammetry of $[Co(bpy)_3]^{3+}/[Co(bpy)_3]^{2+}$ in aqueous solution. The bare $[Co(bpy)_3]^{3+}$ shows similar CV curve with a reversible peak at 0.76 V vs. RHE, which can be assigned to $[Co(bpy)_3]^{3+/2+}$ redox.26 The addition of $[Co(bpy)_3]^{3+}$ does not change the peak position but enhance the redox peak intensity, indicating the $[Co(bpy)_3]^{3+}$ has the same redox pathway with that of $[Co(bpy)_3]^{2+}$. These result indicates the $[Co(bpy)_3]^{3+}$ and $[Co(bpy)_3]^{2+}$ redox can invert each other reversibly, which is of crucial importance in driving electron transfer in this Z-scheme photocatalytic H_2 production system.

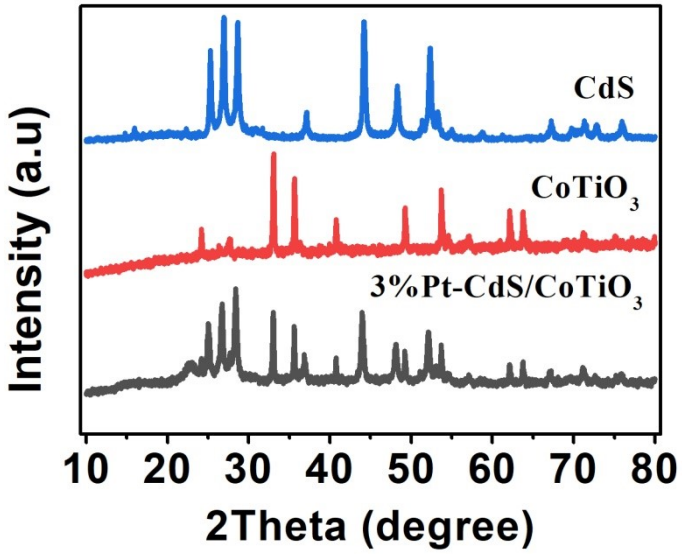

Figure S8. XRD patterns of bare CdS, $CoTiO_3$ and 3%Pt-CdS/$CoTiO_3$ composite collected from photocatalytic reaction solution after 12 h of irradiation.

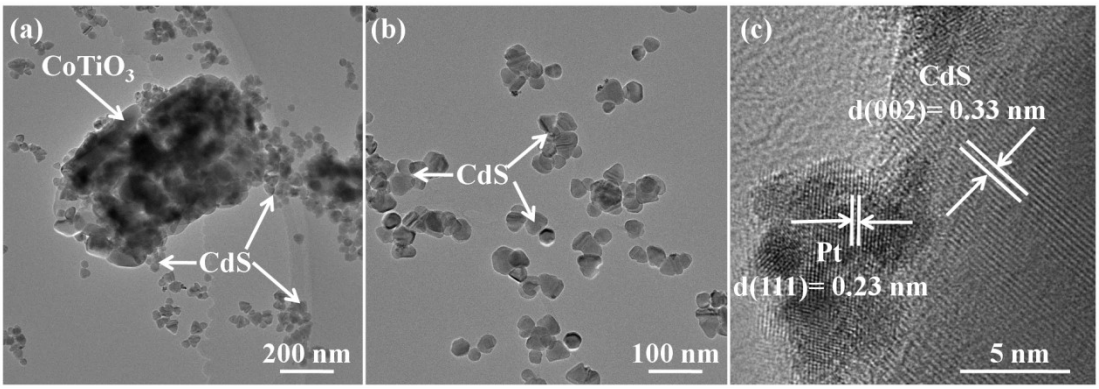

Figure S9. TEM images of 3%Pt-CdS/$CoTiO_3$ composite collected from photocatalytic reaction solution after 12 h of irradiation.

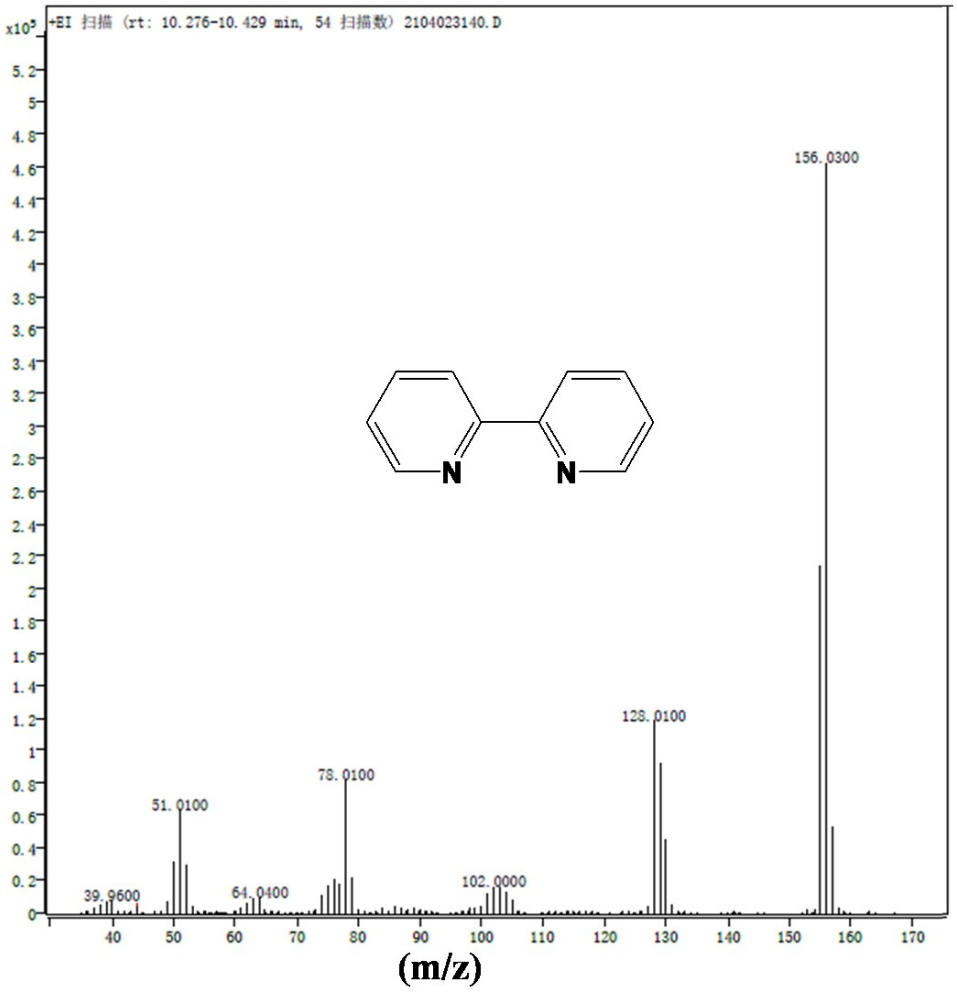

Figure S10. GC-MS of decomposition product collected from the reaction solution after 4 h of irradiation clearly reveal 2,2'-bipyridine dissociate from cobalt complexes (m/z = 156).

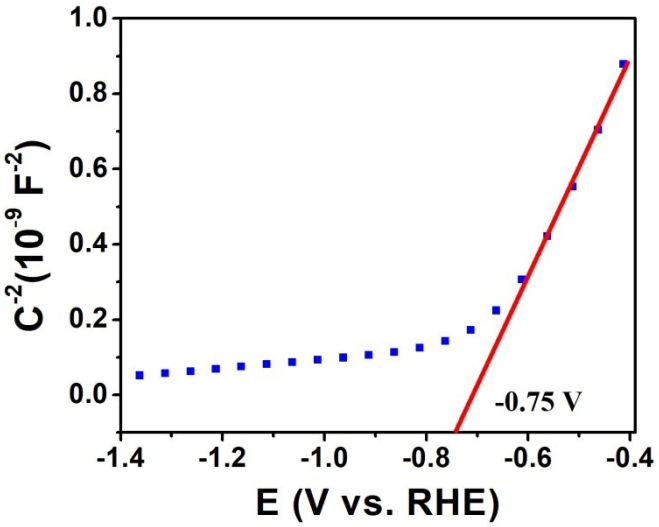

Figure S11. Mott-Schottky plot of CdS electrode measured in neutral 0.5 M Na_2SO_4 aqueous solution.

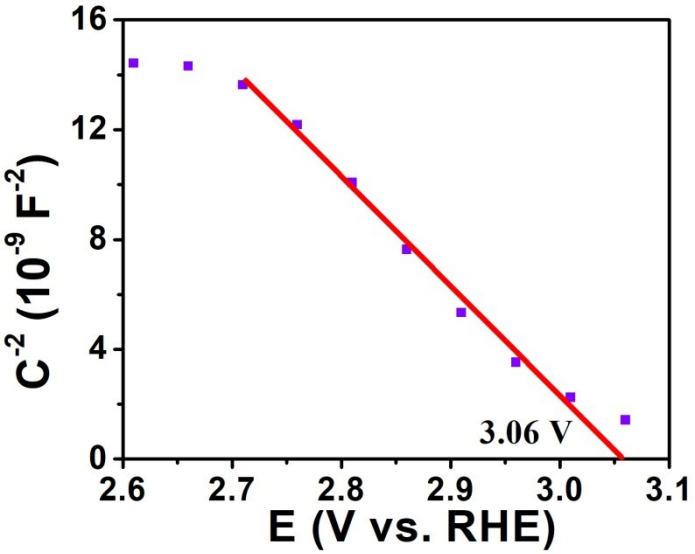

Figure S12. Mott-Schottky plot of $CoTiO_3$ electrode measured in neutral 0.5 M Na_2SO_4 aqueous solution

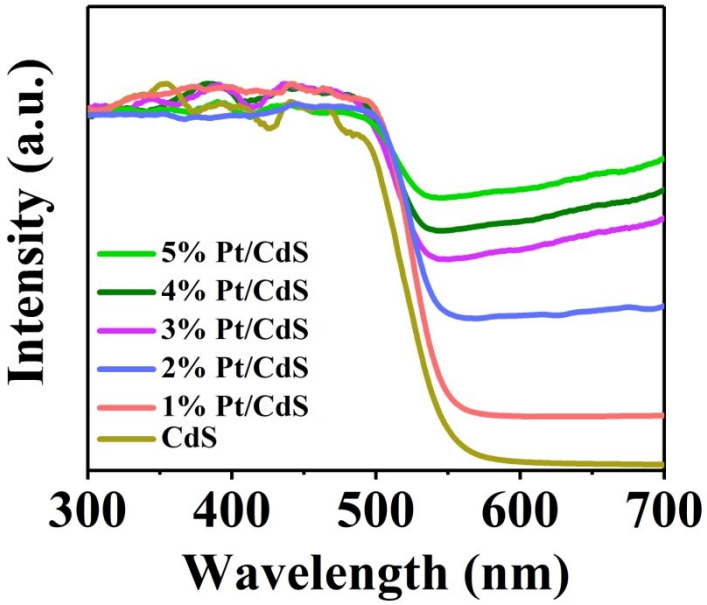

Figure S13. UV-Vis absorption spectrum of Pt/CdS sample.

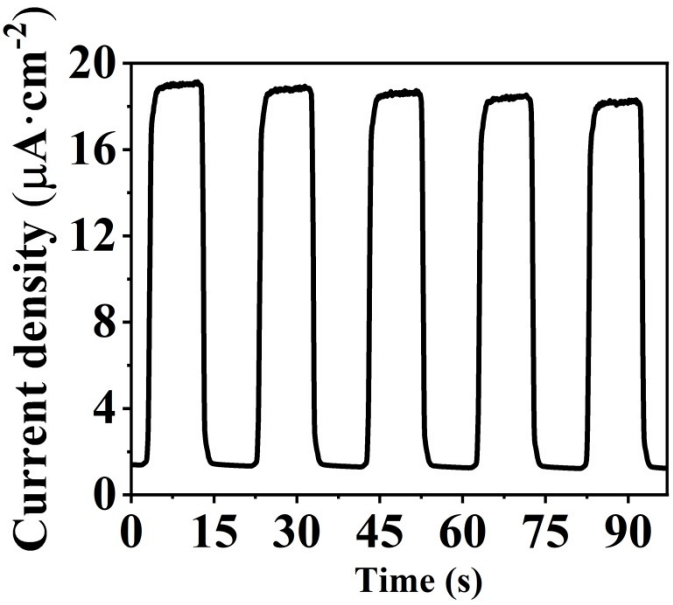

Figure S14. Transient photocurrent response of CdS electrode.

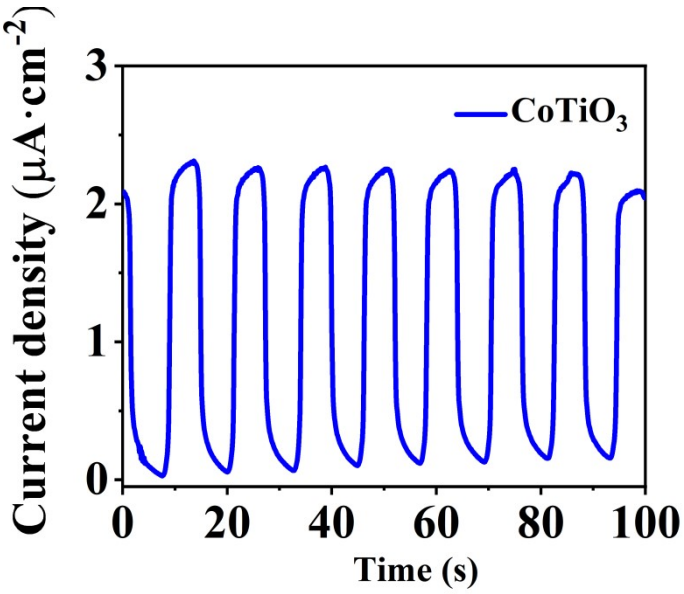

Figure S15. Transient photocurrent response of $CoTiO_3$ electrode.

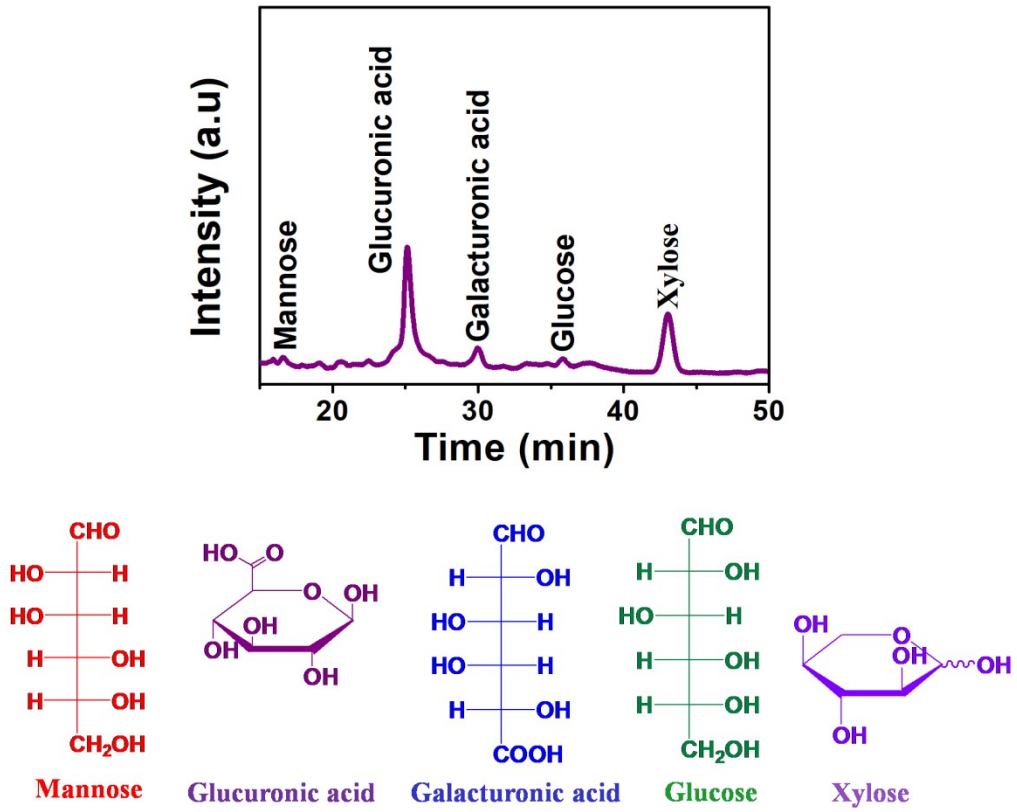

Figure S16. Liquid chromatography analysis for the decomposition products of lignocelluloses after photocatalytic reaction as well as their chemical structures

.

Table S1. Comparison of photocatalytic performance for H2 production between the current work and other reported studies.

Enery	Photocatalyst	Sacrificial reagent.	Light source	H_2 evolution rate ($umol \cdot h^{-1} \cdot g^{-1}$)	AQY(%)	ref
1	Pt/P25	cellulosic	AM 1.5	129	-	1
2	Pt/P25	rice husk suspension	AM 1.5	62.5	-	1
3	CdS/CdO_x	celluloses	AM 1.5	4200	1.2 (430 nm)	2
4	Pt/TiO_2	Cherry wood	Xe lamp	49	1.1	3
5	Pt/P25	celluloses	Xe lamp	~230	-	4
6	MoS_2/TiO_2	celluloses	Xe lamp	201	1.45(380 nm)	5
7	$CdS/CoTiO_3$	celluloses	Xe lamp	106.3	0.47(420 nm)	This work

1. Zhang, N.; Jalil, A.; Wu, D.; Chen, S.; Liu, Y.; Gao, C.; Ye, W.; Qi, Z.; Ju, H.; Wang, C.; Wu, X.; Song, L.; Zhu, J.; Xiong, Y. Refining Defect States in $W_{18}O_{49}$ by Mo Doping: A Strategy for Tuning N_2 Activation towards Solar-Driven Nitrogen Fixation. *J. Am. Chem. Soc.* **2018**, *140*, 9434-9443.
2. Huiqiang Maa,b, Zhenyu Shi a, Shuang Li a, Na Liub,∗Large-scale production of graphitic carbon nitride with outstanding nitrogen photofixation ability via a convenient microwave treatment. Applied Surface Science 379 (2016) 309–315.
3. Li, J.; Wang, D.; Guan, R.; Zhang, Y.; Zhao, Z.; Zhai, H.; Sun, Z. Vacancy-Enabled Mesoporous TiO_2 Modulated by Nickel Doping with Enhanced Photocatalytic Nitrogen Fixation Performance. *ACS Sustainable Chem. Eng*. **2020**, *8*, 18258-18265.
4. A. Caravaca, W. Jones, C. Hardacre, M. Bowker. *Proc. R. Soc. A* 201**6**, **472**: 20160054.
5. P. Wang, Y. J. Yuan, Q. Y. Liu, Q. Cheng, Z. K. Shen, Z. T. Yu, Z. Zou， *ChemSusChem* 2021, **14**, 2860-2865